Princeton Plasma Physics Laboratory

PPPL- 5107

PPPL-5107

Global Modeling of ULF Waves at Mercury

Eun-Hwa Kim, Jay R. Johnson,
Ernest Valeo, and Cynthia K. Phillips

January 2015

Prepared for the U.S. Department of Energy under Contract DE-AC02-09CH11466.

Princeton Plasma Physics Laboratory
Report Disclaimers

Full Legal Disclaimer

Trademark Disclaimer

PPPL Report Availability

Princeton Plasma Physics Laboratory:

http://www.pppl.gov/techreports.cfm

Office of Scientific and Technical Information (OSTI):

http://www.osti.gov/scitech/

Related Links:

U.S. Department of Energy

Office of Scientific and Technical Information

Global Modeling of ULF waves at Mercury

2 Eun-Hwa Kim[1] , Jay R. Johnson[1], Ernest Valeo[2] and Cynthia K. Phillips[2]

4 Corresponding author: E.-H. Kim, Princeton Center for Heliophysics, Princeton Plasma Physics Laboratory, Princeton University, P.O. Box 0451, Princeton, NJ 08543-0451, USA

6 (ehkim@pppl.gov)

[1] Princeton Center for Heliophysics, Princeton Plasma Physics Laboratory, Princeton University, Princeton, New Jersey, USA

[2] Princeton Plasma Physics Laboratory, Princeton University, New Jersey, USA

Abstract

ULF waves in the ion cyclotron frequency range waves have been often observed at Mercury's magnetosphere. Although previous statistical studies have shown that ULF waves are primarily compressional near the equator and transverse with linear polarization at higher latitude, the underlying reason for this distribution of wave polarization has not been understood. In order to address this key question, we have developed a two-dimensional, finite element code that solves the full wave equations in global magnetospheric geometry. Using this code, we show that (1) efficient mode conversion from the fast compressional waves to the ion-ion hybrid resonance occurs at Mercury consistent with previous calculations; (2) such mode-converted waves globally oscillate similar to field-line resonance at Earth; and (3) compressional wave energy is primarily localized near the equator, while field-aligned transverse, linearly polarized waves generated by mode conversion at the ion-ion hybrid resonance radiate to higher latitude. Based on these wave solutions, we suggest that the strong transverse component of observed ULF waves at Mercury in high magnetic latitude can be explained as excitation of the field-line resonant waves at the ion-ion hybrid resonance.

1. Introduction

NASA's Mariner 10 and MESSENGER (MErcury Surface, Space ENvironment, GEochemistry, and Ranging) spacecraft missions provide a wealth of observations within study Mercury's magnetosphere [e.g., *Ness et al.*, 1974, *Slavin et al.*, 2008, 2009, *Anderson et al.*, 2008, 2011], and both spacecraft detected ultra-low frequency (ULF) waves in the ion cyclotron frequency range [*Russell*, 1989; *Boardsen et al.*, 2009a, b, 2012].

A recent statistical study of ULF waves at Mercury based on MESSENGER data [*Boardsen et al.*, 2012] reported the occurrence and polarization of the detected waves. The waves are usually observed between radial distances of 1.1 to 1.8 R_M with maximum occurrence near $R_M \sim 1.4$, where R_M is Mercury's radius (2440km), and between magnetic latitudes of $\pm 40^\circ$ with strong occurrence near the magnetic equator. These waves are also detected primarily on the night side with two maximum peaks around MLT 6 and 21. Measurements of wave polarization indicate that the waves are mostly compressional near the magnetic equator, but the transverse component is dominant at latitudes greater than $\sim 20^\circ$. The transverse fluctuations are also linearly polarized.

The origin of these ULF waves has been of great interest since they were first detected by Mariner 10 [*Russell*, 1989]. Because of their linearly polarization, they were thought to result from field-line resonance in the multiple ion plasmas [e.g., *Russell*, 1989; *Othmer et al.*, 1999; *Glassmeier et al.*, 2003, 2004; *Kim* and *Lee*, 2003; *Klimushkin et al.*, 2006]. However, it was later argued that the waves detected by Mariner 10 are not field-line resonances because the observed waves also have a significant magnetic compressional component [*Blomberg*, 1997; *Southwood*, 1997; *Kim et al.*, 2008].

Field-line resonances at Mercury are expected to occur at the ion-ion hybrid (IIH) resonances and should have purely transverse polarization [*Kim et al.*, 2008]. When incoming fast compressional waves (FWs) match the IIH resonance condition, strong absorption of incoming FWs can occur leading to excitation of the IIH resonance [e.g., *Karney et al.*, 1979]. Numerical simulations in slab coordinates showed that this mode-converted IIH waves are guided by the ambient magnetic field line ($\mathbf{B}_0$) and have linear polarization [*Kim et al.*, 2008, 2011, 2013]. However, the simulations did not describe the two-dimensional magnetic curvature effect, which can separate the regions of compressional wave dominance from regions dominated by the global transverse mode converted wave.

Similar to *Kim et al.* [2008], *Boardsen et al.* [2012] also concluded that the bulk of the wave observations from MESSENGER cannot be explained by ion cyclotron waves or field-line resonance because of high compressibility of the detected waves near the magnetic equator. Instead, they proposed that the observed waves could be mainly composed of short wavelength (~100 km) electromagnetic ion Bernstein mode waves (IBWs) in a high β proton plasma. Using ray tracing calculations, they confirmed that electromagnetic IBWs generated by loss cone instability can explain MESSENGER observations where the compression straddles the equator [*Boardsen et al.*, 2014]. Although the IBWs in the ray tracing calculations can exhibit transverse polarization off the equator, they reflect at magnetic latitudes around 12°, which is much less than typically observed (most dominant at 20° extending up to 40°).

Therefore, a key question that remains concerning ULF waves at Mercury is why the waves are primarily compressional near the equator and transverse with linear polarization at higher latitude. If the waves are driven by the same source, does the polarization change because of propagation effects or because of mode conversion processes? In order to address these questions,

we have developed a two-dimensional full wave code using the finite element method and unstructured triangle mesh, which has been used to examine general plasma waves in Tokamak [e.g., *Brambilla*, 1999] and field-line resonances in the magnetosphere [e.g., *Lu et al.*, 2003]. The code we developed describes three-dimensional wave structure including mode conversion when plasma waves are launched in two-dimensional axisymmetric background plasma with arbitrary magnetic field topology. Using the newly developed wave code, we examine ULF waves at Mercury that have been detected inside Mercury's magnetosphere by Mariner 10 and MESSENGER spacecraft.

2. Two-Dimensional Full Wave Code

We utilize a two-dimensional, finite element code that solves the full wave equations in global magnetospheric geometry. Assuming a time dependence $\exp(-i\omega t)$, where ω is an angular frequency, the linear and cold plasma wave equation takes the form,

$$\nabla\times\nabla\times\mathbf{E}-\frac{\omega^2}{c^2}\boldsymbol{\varepsilon}\cdot\mathbf{E}=4\pi i\frac{\omega}{c^2}\mathbf{J}_{ext}, \tag{1}$$

where $\mathbf{E}$ is the perturbed electric field, $\mathbf{J}_{ext}$ is the (localized) external current source launching the waves within our model, $\boldsymbol{\varepsilon}$ is the dielectric tensor, which is expressed in coordinates aligned along and across the local $\mathbf{B}_0$ direction,

$$\boldsymbol{\varepsilon}=\varepsilon_S(\mathbf{I}-\hat{\mathbf{b}}\hat{\mathbf{b}})+i\varepsilon_D\mathbf{I}\times\hat{\mathbf{b}}+\varepsilon_P\hat{\mathbf{b}}\hat{\mathbf{b}}, \tag{2}$$

where $\hat{\mathbf{b}}=\mathbf{B}_0/|\mathbf{B}_0|$ and $\varepsilon_{S,D,P}$ are dispersion functions defined by *Stix* [1992]. Because wave Eqs. (1)-(2) include all electron and ion effects, the code enables us to study a wide range of fluid waves from MHD waves to Langmuir oscillations in a consistent manner when the system is arbitrarily inhomogeneous, but in this paper we confine our study to wave in the ion cyclotron frequency range.

In this frequency range, typically $\varepsilon_P >> \varepsilon_{S(D)}$ and $E_\perp >> E_\parallel$, where subscript $\parallel(\perp)$ is along (perpendicular) to $\mathbf{B}_0$, so accurately capture this disparity, the field is represented in terms of its projections along and perpendicular to $\mathbf{B}_0$. We pick a local orthogonal basis ($\hat{\mathbf{b}}, \hat{\boldsymbol{\varphi}}, \hat{\boldsymbol{\eta}}$), where the unit vector $\hat{\mathbf{b}}$ is along the magnetic field line from north to south, $\hat{\boldsymbol{\varphi}}$ is the azimuthal direction and $\hat{\boldsymbol{\eta}}$ is normal to the field line pointing outward ($\hat{\boldsymbol{\eta}} = \hat{\mathbf{b}} \times \hat{\boldsymbol{\varphi}}$), with the assumption of $\mathbf{B}_0 \cdot \hat{\boldsymbol{\varphi}} = 0$, appropriate for a 2D model with azimuthal symmetry.

Eq. (1) can then be expressed in cylindrical coordinates $(\hat{\mathbf{r}}, \hat{\mathbf{z}}, \hat{\boldsymbol{\varphi}})$ with

$$E = \sum_m \left(E_b^m \hat{\mathbf{b}} + E_\eta^m \hat{\boldsymbol{\eta}} + E_\varphi^m \hat{\boldsymbol{\varphi}} \right) \exp(im\varphi), \tag{3}$$

where m are azimuthal wavenumbers. For a dipole field, $\hat{\mathbf{b}} \equiv 3\sin\theta\cos\theta\,\hat{\mathbf{r}} + (3\cos^2\theta - 1)\hat{\mathbf{z}}$, where $\cos\theta = z/\sqrt{r^2 + z^2}$.

In order to adapt to multiple singular lines, we solve Eq. (1) on an unstructured triangular mesh. We represent the variation of the field within each triangle by vertex-based linear finite elements local basis function, $F_{j,k}$, where j labels each triangle and k = 1, 2, 3 labels each of its vertices. That is, $F_{j,k}$ varies linearly between 1 at vertex k^{th} and 0 at the other vertices, and is identically 0 outside triangle j. Since we assume axisymmetry in the azimuthal direction, thus the electric field is represented as:

$$E(r,z)\exp(im\varphi) = \sum_{j,k} E_{j,k} F_{j,k}(r,z)\exp(im\varphi). \tag{4}$$

Eq. (4) is cast into matrix form by taking its inner product in turn with each $F_{j,k}$, and integrating over the whole plasma volume by parts to obtain the weak variational form [e.g., *Brambilla*, 1999],

$$\int d\varphi\, r dr\, dz \left\{ \left(\nabla \times \mathbf{F}_{j,k}\right) \cdot \left(\nabla \times \mathbf{E}\right) + \mathbf{F}_{j,k} \cdot \boldsymbol{\varepsilon} \cdot \mathbf{E} + i \frac{\omega}{c^2} \mathbf{F}_{j,k} \cdot \mathbf{J}_{ext} \right\} = 0 \,. \tag{5}$$

Substitution of Eq. (4) into Eq. (5) yields a sparse matrix system that is amenable to solution by standard algorithms.

One advantage of using the finite element method is that the local basis functions can be readily adapted to boundary shapes [e.g., *Lu et al.*, 2003] and can be packed in such a way as to provide higher resolution in regions where solutions may exhibit singular behavior. In order to generate magnetospheric geometry, we have adapted the DISTMESH algorithm [*Persson and Strang*, 2004]. The algorithm constructs a 2D triangular given a specified boundary and a target density function. The density of the mesh can be specified based on the expected wavelength obtained from solution of the local dispersion, except close to resonances, so that the most efficient resolution is used.

3. Wave Solutions at Mercury's magnetosphere

As shown in Figure 1, we adopt Mercury's dipole field model by assuming the magnetic field strength at Mercury's surface is $3.1\times10^{-7}\,\mathrm{T}$ [*Anderson et al.*, 2008]. Because sodium is one of the major heavy ions at Mercury [e.g., *Zurbuchen et al.*, 2008, 2011; *Raines et al.*, 2013, 2014], similar to previous numerical studies [*Kim et al.*, 2008, 2011] we adopt an electron-proton-sodium plasma with constant electron density ($N_e = 1\mathrm{cm}^{-3}$) and sodium concentration ratio ($\eta_{Na} = N_{Na}/N_e = 15\%$).

We solve Eq. (1) in the domain as $0 < r/\mathrm{R_M} < 2.5$ and $-2 < z/\mathrm{R_M} < 2$ as shown in Figure 1 and Eq. (1) using absorbing boundary conditions (which only allows outgoing wave solutions) at the edge of the solution domain except at Mercury's surface, which is assumed to be a perfect conductor leading to wave reflection. In this calculation, for simplicity, the azimuthal wave

number *m* of the source is assumed to be 0. Although for an Alfven resonance, *m* = 0 would not allow mode conversion, when heavy ions are present, mode conversion can still occur even for *m* = 0.

Similar to the waves detected at Mercury, we select wave frequency of f = 0.95 Hz (thus $\omega = 2.98\text{Hz}$) near $(r_{ext}, z_{ext}) = (2\text{R}_\text{M}, 0)$ with

$$\mathbf{J}_{ext} = \left[\exp\left(-(r - r_{ext})/\Delta r_{ext}\right) + \exp\left(-(z - z_{ext})/\Delta z_{ext}\right)\right](\hat{\eta} - i\hat{\varphi}), \quad (6)$$

where $\Delta r_{ext} = 0.125\,\text{R}_\text{M}$ and $\Delta z_{ext} = 0.25\,\text{R}_\text{M}$, respectively. Based on the wavelength of dispersion relation of (a) left-handed polarized waves ($n_\parallel^2 = \varepsilon_L$), (b) IIH waves ($n_\parallel^2 = \varepsilon_S$) propagating along $\mathbf{B}_0$, and (c) fast wave modes ($n_\parallel^2 = \varepsilon_L\varepsilon_R/\varepsilon_S$) propagating perpendicular to $\mathbf{B}_0$, we generate the triangle mesh producing 43349 nodes and 85702 triangles. The computing time is approximately 450 seconds CPU time to obtain a solution.

The dispersion relation of FW modes can be written as

$$n_\perp^2 \cong \frac{(\varepsilon_R - n_\parallel^2)(\varepsilon_L - n_\parallel^2)}{(\varepsilon_S - n_\parallel^2)}. \quad (7)$$

Eq. (7) exhibits two cutoffs at $n_\parallel^2 = \varepsilon_{R(L)}$, thus when FW modes propagate perpendicular to $\mathbf{B}_0$ (i.e., $n_\parallel^2 = 0$), the FW modes partially reflect where $\varepsilon_L(\omega = \omega_L) = 0$ or $\varepsilon_R(\omega = \omega_R) = 0$. Eq. (7) also has a resonance where,

$$n_\parallel^2 = \varepsilon_S, \quad (8)$$

which is called the IIH resonance because it occurs between the two ion cyclotron frequencies. When Eq (8) is satisfied, mode conversion from FW modes to IIH resonance occurs and the mode-converted IIH waves propagate along $\mathbf{B}_0$ with dispersion relation of $n_\parallel^2 = \varepsilon_S$. As the mode converted wave propagates to higher magnetic latitude, these waves are partially reflected where

154 $\varepsilon_S(\omega = \omega_{bb}) = 0$ [*Johnson et al.*, 1995; *Johnson and Cheng*,1999; *Kim et al.*, 2009], where ω_{bb} is the Buchsbaum resonance frequency [*Buchsbaum*, 1960].

156 Figure 2 shows the wave solutions of the fluctuating electric (**E**) and magnetic (**B**) fields. In this figure, both the FW and the mode-converted IIH resonant wave modes are clearly seen. The 158 FW mode is directly launched near (r_{ext}, z_{ext}) and propagates to the inner/outer magnetosphere. This wave mode appears in all electric and magnetic field components. Because the FW mode is 160 launched near the magnetic equator as marked "A" in Figure 2b, the waves propagating to inner magnetosphere partially reflect near $r/\mathrm{R_M} = 1.43$, where $\omega = \omega_L$ (as marked "B" in Figure 2b) 162 The rest of the energy penetrates deep into the magnetosphere and totally reflects at Mercury's surface due to the reflecting boundary condition. The FWs reflected from Mercury's surface 164 propagate to the outer magnetosphere with different propagation angle (as marked "C" in Figure 2b), and are eventually absorbed near the outer boundary.

166 The IIH resonant waves appear only in E_η, E_b, and B_φ in Figure 2 showing long wavelength in the $\hat{\mathbf{b}}$ direction and fine structure in the $\hat{\boldsymbol{\eta}}$ direction for $1.4 \leq L_M \leq 1.8$, where L_M is Mercury's L-168 shell, which is consistent with *Kim et al.* [2015] Because the waves launched at $L_M = 2$ are pure FW modes, the waves showing field-aligned structures in E_η and B_φ are unmistakable evidence 170 of mode conversions.

These waves also show a wide range of field-aligned harmonic numbers that increase with 172 along L_M. For instance, the fundamental and 3rd harmonics are seen at $L_M \sim 1.5$ and 1.7, respectively. These results are predicted by previous 1D full wave calculations. *Kim et al.* [2011] 174 showed when the plasma contains 10-17% sodium at $L_M = 1.5$, strong absorption of the FW mode occurs in fundamental wave modes, which is consistent with 2D results. They also show

176 that the wave frequency with higher field-aligned harmonic numbers has stronger absorption at a single magnetic field line when the plasma contains a higher concentration of heavy ions.

178 In Figure 2, we also over-plot the locations where $\omega = \omega_{bb}$, which corresponds to the cutoff of the field-aligned propagation mode-converted waves. Waves in higher L_M encounter the cutoff 180 location before they reach the ground, but because of the wavelength and power are enough large the to penetrate the evanescent region between Buchsbaum resonance to the ground, we found 182 wave power near the surface. Therefore, the IIH resonant waves globally oscillate along the magnetic field-line similar to the field-line resonance at Earth [e.g., *Lee and Lysak*, 1989]. 184 Conversely, field-line resonances occur at Mercury when the IIH resonance conditions are satisfied [e.g., *Kim et al.*, 2008] and because such resonances globally oscillates, they reach 186 higher magnetic latitudes.

In Figure 3, the Poynting flux (**S**) is also calculated in order to examine the flow of wave 188 energy. Because the FW mode is launched near the magnetic equator at $L_M = 2$, S_η shows most of the FW energy propagates toward the inner magnetosphere for $L_M<2.0$ and the outer 190 magnetosphere for $L_M>2.0$. Near L_M =1.43, the FW cutoff is clearly seen in the drop off Poynting flux but because wave power is strong enough to tunnel through the evanescent region, 192 the rest of FW energy reflects at the surface as we expected in Figure 2. The reflected waves also propagate outward at higher latitude. It is noted that spatial structure of S_η are same as the FW 194 structure shown in E_η and E_b. On the other hand, S_b clearly shows the fine structure of field-aligned IIH wave modes. Because the FW energy launched at the magnetic equator, wave energy 196 clearly flows poleward, but because IIH waves reflect near the surface, equatorward energy flow is also seen near L_M =1.6 and 1.9.

198 Based on eigenmode solution shown in Figure 2, we reproduce the time-dependent wave solutions, such as,

200 $$E(r,z,t) = E(r,z)\exp(-i\omega t), \quad (9)$$

as shown in Media 1. The Media 1 clearly shows how FW and mode-converted IIH waves 202 propagates in time.

4. Discussion and Summary

204 In this letter, we utilized a two-dimensional wave code in multi-fluid plasmas that solves the full wave equations in global magnetospheric geometry. Because this wave code adopts a finite 206 element method and unstructured triangle mesh, it provides good resolution of plasma waves in planetary magnetospheres where mode conversion is expected to occur.

208 Using this code, we showed how field-aligned propagating ULF waves at Mercury can be generated by externally driven FWs via mode conversion at the ion-ion hybrid resonance. 210 Consistent with the previous real time simulations in slab geometry [*Kim et al.*, 2008, 2013], the mode-converted IIH waves are strongly guided by $\mathbf{B}_0$ and have linear polarization in E_μ and B_φ. 212 Although the IIH waves are partially reflected at the Buchsbaum resonance at higher magnetic latitude, these waves penetrate the wave stop gap and globally oscillate. Thus the IIH waves can 214 propagate to magnetic latitudes over 40° for realistic magnetic field and densities at Mercury. These results are consistent with the observed waves that can propagate over magnetic latitude of 216 40° with strong magnetic transverse component [*Boardsen et al.*, 2012].

Some wave events detected by MESSENGER often have a narrow frequency band near 1 Hz 218 in a wide range of L-shell. For instance, waves with 1Hz are observed in $1.3 < L_M < 1.8$ and $0 <$ MLT $< 42°$ as shown in Figure 4 from *Boardsen et al.* [2012]. This observation is consistent with

220 the finite element calculation, which the IIH waves with a single wave frequency in a wide range of L shell ($1.4<L_M<1.8$).

222 The simulations also show that field-aligned harmonic number increases along with L-shell with consistency to 1D full wave calculations. *Kim et al.* [2011, 2015] estimated the efficiency of 224 mode conversion of radially propagating FWs at the IIH resonance using a simplified 1D slab cold plasma model that captures the essential features of the IIH resonance. In particular, *Kim et* 226 *al.* [2015] showed that a relatively large absorption occurs in wide range of heavy ion density concentration ratios. Unfortunately these results then suggest that the heavy ion density 228 concentration ratio at Mercury cannot be simply inferred from the frequency of field-aligned IIH waves as previous suggested [*Kim et al.*, 2008; *Kazakov* and *Fülöp*, 2013].

230 Although we obtained general characteristics of FLR at Mercury, there are several limitations in our work. First, we adopt a cold plasma model even though kinetic effects in hot plasmas are 232 believed to be important for the generation and propagation of ULF waves at Mercury [e.g., *Glassmeier et al.*, 2003; *Slavin et al.*, 2009; *Boardsen et al.*, 2012, 2014]. In hot plasmas, the FW 234 mode can be converted into the short wavelength ion Bernstein wave (IBW) or ion cyclotron wave (ICW) modes (or their higher harmonics) at the IIH resonance [e.g., *Wukitch et al.*, 2005]. 236 The mode-converted IBW modes have short-wavelength in the radial direction and long-wavelength in field-aligned direction, thus the mode-converted IBW mode is expected to 238 propagate at large normal angle because of $k_\perp >> k_\parallel$. Therefore, a short wavelength IBW mode at Mercury could be either externally generated via mode conversion at the IIH resonance or 240 internally generated from plasma instability [*Boardsen et al.*, 2014]. It should be noted that the wave occurrence is much higher near the magnetic equator than off the equator and wave 242 characteristics at higher latitude are mainly transverse while near the equator the waves are

strongly compressible. Thus the compressionally dominant waves near the magnetic equator could be mixed with internally generated and externally mode-converted IBW modes while waves at higher magnetic latitudes could be mode-converted IIH waves (or IBWs).

Second, we assume electron-hydrogen-sodium plasmas and a constant sodium density for simplicity. When lighter ions, such as He^{+} and He^{++}, are included in Mercury's magnetosphere, the cutoff condition of the field-aligned waves, such as the Buchsbaum resonance, shift toward the outer magnetosphere and lower magnetic latitude. In addition, depending on the heavy ion density ratios, the wave stop gap between the locations where $\omega = \omega_{bb}$ and $\omega = \omega_{ci}$ becomes wider or narrower [*Kim et al.*, 2015]. Thus the mode-converted waves can be tunnel through the wave stop gap similar to left-handed polarized EMIC waves at Earth [*Johnson et al.*, 1989, 1995, *Johnson and Cheng*, 1999] or localized between Buchsbaum locations [*Kim et al.,* 2009] depending on wave tunneling effects.

Finally, we adopt a simple dipole magnetic field model with a perfectly conducting boundary condition at Mercury's surface rather than realistic magnetic configurations [e.g., *Anderson et al.*, 2008, 2010, 2011] or conductivity [*Anderson et al.*, 2014]. Because the boundary condition with finite conductivity can damp the field-line resonance at Earth [*Lee and Takahashi*, 2006], the realistic boundary condition might be important in Mercury's magnetosphere and these subject will be left as future work.

Acknowledgements. The work at the Princeton University was supported by NASA grants (NNH09AM53I, NNH09AK63I, and NNH11AQ46I), NSF grant ATM0902730, and DOE contract DE-AC02-09CH11466.

References

266 Anderson, B. J., M. H. Acuna, A. Korth, C. L. Purucker, C. L. Johnson, J. A. Slavin, Solomon S. C. and R. L. McNutt (2008), The structure of Mercury's magnetic field from
268 MESSENGER's first flyby, *Science* 321, 82-85.

Anderson, B. J., M. H. Acuna, H. Korth, J. A. Slavin, H. Uno, C. L. Johnson, M. E. Purucker,
270 Solomon S. C., J. M. Raines, T. H. Zurbuchen, G. Gloeckler and R. L. McNutt Jr. (2010), The Magnetic Field of Mercury, *Space Sci. Rev. 152*, 307–339, doi:10.1007/s11214-009-
272 9544-3.

Anderson, B. J., C. L. Johnson, H. Korth, M. E. Purucker, Winslow R. M., J. A. Slavin, Solomon
274 S. C., R. L. McNutt Jr., J. M. Raines and T. H. Zurbuchen (2011), The Global Magnetic Field of Mercury from MESSENGER Orbital Observations, Science 333, 1859-1862, doi:
276 10.1126/science.1211001.

Anderson, B. J., C. L. Johnson, H. Korth, J. A. Slavin, Winslow R. M., R. J. Phillips, R. L.
278 McNutt Jr. and Solomon S. C. (2014), Steady-state field-aligned currents at Mercury, *Geophys. Res. Lett. 41*, 7444–7452, doi:10.1002/2014GL061677.

280 Blomberg, L. G. (1997), Mercury's magnetosphere, exosphere and surface : low-frequency field and wave measurements as a diagnostic tool, Planet. Space Sci. 45, 143-148.

282 Boardsen, S. A., B. J. Anderson, M. H. Acuna, J. A. Slavin, H. Korth and Solomon S. C. (2009a), Narrow-band ultra-low-frequency wave observations by MESSENGER during its
284 January 2008 flyby through Mercury's magnetosphere, *Geophy. Res. Lett. 36*, L01104.

Boardsen, S., J. A. Slavin, B. J. Anderson, A. Korth and Solomon S. C. (2009b), Comparison of ultra-low-frequency waves at Mercury under northward and southward IMF, *Geophy. Res. Lett. 36*, L18106.

Boardsen, S. A., S. A. Slavin, B. J. Anderson, H. Korth, D. Schriver and Solomon S. C. (2012), Survey of coherent ~1 Hz waves in Mercury's inner magnetosphere from MESSENGER observations, *J. Geophys. Res. 117*, A00M05, doi:10.1029/2012JA017822.

Boardsen, S., E.-H. Kim, J. M. Raines, J. A. Slavin, D. J. Gershman, B. J. Anderson, H. Korth, T. Sundberg, D. Schriver, P. Travnicek and S. C. Solomon (2014), Ray-tracing of the ion Bernstein mode in moderately high proton beta ~0.1 in Mercury's inner magnetosphere, *J. Geophysics. Res.*, submitted

Brambilla, M. (1999), Numerical simulation of ion cyclotron waves in tokamak plasmas, *Plasma Phys. Control. Fusion 41*, 1.

Buchsbaum, S. J. (1960), Ion Resonance in a Multicomponent Plasma, *Phys. Rev. Lett 5*, 495-497.

Glassmeier, K.-H., P. N. Mager and D. Y. Klimushkin (2003), Concerning ULF pulsations in Mercury's magnetosphere, *Geophys. Res. Lett. 30*, 1928.

Glassmeier, K.-H., D. Klimushkin, C. Othmer, P. Mager (2004), ULF waves at Mercury: Earth, the giants, and their little brother compared, *Adv. Space Res.* 33, 1875-1883, doi:10.1016/j.asr.2003.04.047.

Johnson, J. R., T. Chang, G. B. Crew, and G. B. Crew (1989), Equatorially generated ULF waves as a source for the turbulence associated with ion, Geophys. Res. Lett., 16, 1469-1472, doi: 10.1029/GL016i012p01469.

Johnson, J. R., T. Chang, and G. B. Crew (1995), A study of mode conversion in an oxygen-
308 hydrogen plasma, Phys. Plasmas, 2, 1274–1284.

Johnson, J. R. and C. Z. Cheng (1999), Can ion cyclotron waves propagate to the ground?,
310 *Geophys. Res. Lett. 26*, 671-674.

Karney, C. F. F., F. W. Perkins and Sun Y. C. (1979), Alfven resonance Effects on
312 Magnetosonic Modes in Large Tokamaks, *Phys. Rev. Lett. 24*, 1621.

Kazakov, Y. O. and T. Fülöp (2013), Mode Conversion of Waves in the Ion-Cyclotron
314 Frequency Range in Magnetospheric Plasmas, *Phys. Rev. Lett. 111*, 125002.

Kim, E.-H. and D.-H. Lee (2003), Resonant absorption of ULF waves near the ion cyclotron
316 frequency: A simulation study, *Geophys. Res. Lett. 30*, 2240.

Kim, E.-H., J. R. Johnson and D. H. Lee (2008), Resonant absorption of ULF waves at Mercury's
318 magnetosphere, *J. Geophys. Res. 113*, A11207.

Kim, E.-H., J. R. Johnson and K.-D. Lee (2011), ULF wave absorption at Mercury, *Geophys.*
320 *Res. Lett. 38*, L16111, doi:10.1029/2011GL048621.

Kim, E.-H., J. R. Johnson, I. H. Ciarns and D.-H. Lee (2009), Waves in space plasmas, *RADIO*
322 *FREQUENCY POWER IN PLASMA: Proceedings of the 18th Topical Conference 1187*, 13,
doi:10.1063/1.3273713.

324 Kim, E.-H., J. R. Johnson, D.-H. Lee and Y. S. Pyo (2013), Field-line resonance structure in
Mercury's multi-ion magnetosphere, *Earth, Planets, and Space 65*, 447.

326 Kim, E.-H., S. A. Boardsen, J. R. Johnson and J. A. Slavin (2015), ULF waves at Mercury, in
Low-Freqeucny Waves in Space Plasmas (eds A. Keiling, D.-H. Lee, K.-H. Glassmeier, and
328 M. N. Valery), American Geophysical Union, Washington, D. C., submitted.

Klimushkin, D. Y., P. N. Mager and K.-H. Glassmeier (2006), Axisymmetric Alfven resonances in a multi-component plasma at finite ion gyrofrequency, *Ann. Geophys. 24*, 1077-1084.

Lee, D.-H. and K. Takahashi (2006), MHD Eigenmodes in the Inner Magnetosphere, in *Magnetospheric ULF Waves: Synthesis and New Directions* (eds K. Takahashi, P. J. Chi, R. E. Denton and R. L. Lysak), American Geophysical Union, Washington, D. C., doi: 10.1029/169GM07

Lee, D.-H. and R. L. Lysak (1989), Magnetospheric ULF wave coupling in the dipole model - The impulsive excitation, *J. Geophys. Res. 94*, 17097-17103.

Lu, J. Y., R. Rankin, R. Marchand, V. T. Tikhonchuk and J. Wanliss (2003), Finite element modeling of nonlinear dispersive field line resonances: Trapped shear Alfven waves inside field-aligned density structures, *J. Geophys. Res*. 108, 1394, doi:10.1029/2003JA010035.

Ness, N. F., K. W. Behannon, R. P. Lepping, Y. C. Whang and K. H. Schatten (1974), Magnetic field observations near Mercury: Preliminary results from Mariner 10, *Science* 185, 151-160.

Othmer, C., K.-H. Glassmeier and R. Cramm (1999), Concerning field line resonances in Mercury's magnetosphere, *J. Geophys. Res. 104*, 10369-10378.

Persson, P.-O. and G. Strang (2004), A Simple Mesh Generator in MATLAB., *SIAM Review 46*, 329.

Raines, J. M., D. J. Gershman, J. A. Slavin, T. H. Zurbuchen, H. Korth, B. J. Anderson and Solo (2014), Structure and dynamics of Mercury'smagnetospheric cusp: MESSENGER measurements of protons and planetary ions, *J. Geophys. Res 119*, 6587–6602, doi:10.1002/2014JA0201.

Raines, J. M., D. J. Gershman, T. H. Zurbuchen, M. Sarantos, J. A. Slavin, J. A. Gilbert, H. Korth, B. J. Anderson, G. Gloeckler, S. M. Krimigis, D. N. Baker, R. L. McNutt and S. C. Solomon (2013), Distribution and compositional variations of plasma ions in Mercury's space environment: The first three Mercury years of MESSENGER observations, J. Geophys. Res. 118, 1604-1619, doi:10.1029/2012JA018073.

Russell, C. T. (1989), ULF waves in the Mercury magnetosphere, *Geophys. Res. Lett. 16*, 1253-1256.

Slavin, J. A., M. H. Acu, B. J. Anderson, D. N. Baker, M. Benna, G. Gloeckler, R. E. Gold, G. C. Ho, R. M. Killen, H. Korth, S. M. Krimigis, R. L. McNutt, L. R. Nittler, J. M. Raines, D. Schriver, S. C. Solomon, R. D. Starr, P. Tr and T. H. Zurbuchen (2008), Mercury's Magnetosphere After MESSENGER's First Flyby, Science 321, 85-.

Slavin, J. A., M. H. Acuna, B. J. Anderson, D. N. Baker, M. Benna, S. A. Boardsen, G. Gloeckler, R. E. Gold, G. C. Ho, H. Korth, S. M. Krimigis, R. L. McNutt, J. M. Raines, M. Sarantos, D. Schriver, S. C. Solomon, P. Travnicek and T. H. Zurbuchen (2009), MESSENGER Observations of Magnetic Reconnection in Mercury’s Magnetosphere, *Science 324*, 606-610, doi:10.1126/science.1172011.

Southwood, D. J. (1997), The magnetic field of Mercury, *Plane 45*, 113-117.

Stix, T. H., 1992. *Waves in plasmas*. New York,: American Institute of Physics.

Wukitch, S. J., Y. Lin, A. Parisot, J. C. Wright, P. T. Bonoli, M. Porkolab, N. Basse, E. Edlund, A. Hubbard, L. Lin, A. Lynn, E. Marmar, D. Mossenssian, P. Phillips and G. Sshilling (2005), on cyclotron range of frequency mode conversion physics in Alcator C-Mod: Experimental measurements and modeling, *Phys. Plasmas 12*, 056104.

372 Zurbuchen, T. H., J. M. Raines, G. Gloeckler, S. M. Krimigis, J. A. Slavin, P. L. Koehn, R. M. Killen, A. L. Sprague, R. L. McNutt Jr. and Solomon S. C. (2008), MESSENGER
374 Observations of the Composition of Mercury's Ionized Exosphere and Plasma Environment, *Science 321*, 90-92.

376 Zurbuchen, T. H., J. M. Raines, J. A. Slavin, D. J. Gershman, J. A. Gilbert, G. Gloeckler, B. J. Anderson, D. N. Baker, H. Korth, Krimigis S. M., Sarantos M. S., Schiriver D., R. L. McNutt
378 Jr. and Solomon S. C. (2011), MESSENGER Observations of the Spatial Distribution of Planetary Ions Near Mercury, *Science 333*, 1862-1865, doi: 10.1126/science.1211302.

380

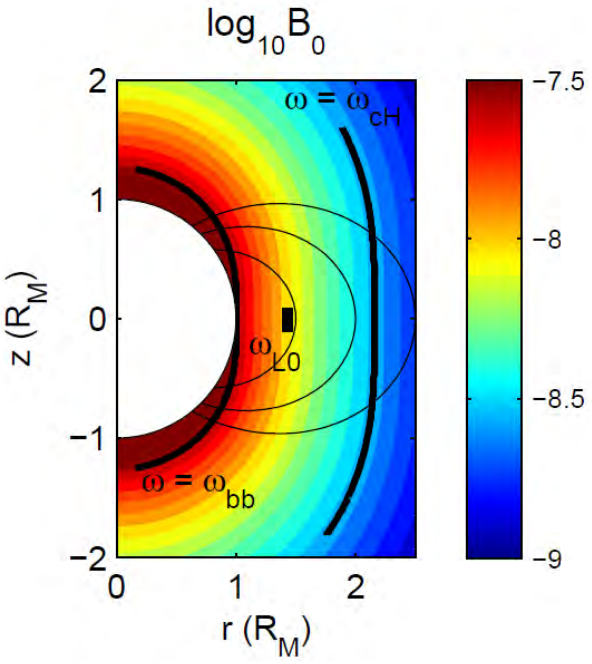

382

384 Figure 1. The ambient magnetic field (B_0) in logarithm scale. Here, two solid lines are the proton cyclotron resonance location where $\omega=\omega_{ci}$ and ω_{ci} is proton gyro frequency, and Buchsbaum

386 resonance location where $\omega=\omega_{bb}$ and ω_{bb} is Buchsbaum resonance frequency. ω_{L0} represent the FW wave cutoff locations at the magnetic equator.

388

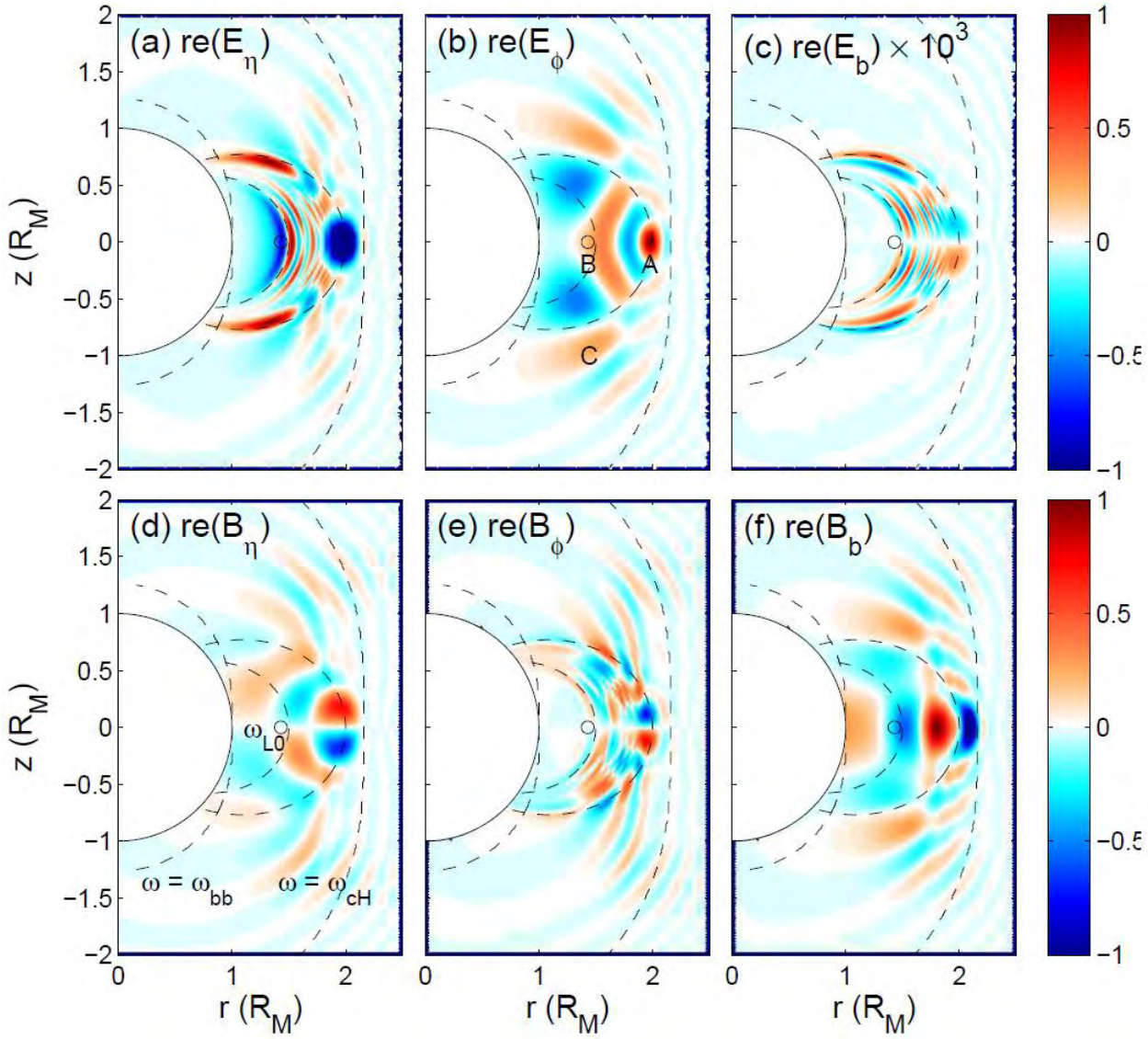

Figure 2. Wave solutions if (a-c) electric field and (d-f) magnetic field. Here, $\hat{\mathbf{b}}$ is along the magnetic field line from north to south, $\hat{\boldsymbol{\varphi}}$ is the usual azimuthal direction and $\hat{\boldsymbol{\eta}}$ is normal to the field line pointing outward ($\hat{\boldsymbol{\eta}} = \hat{\mathbf{b}} \times \hat{\boldsymbol{\varphi}}$), with the assumption of $\mathbf{B}_0 \cdot \hat{\boldsymbol{\varphi}} = 0$. The dashed lines are where $\omega=\omega_{ci}$ and $\omega=\omega_{bb}$, or field line at L_M=1.5 and 2.0, respectively. The circle represent $\omega=\omega_{L0}$, the FW wave cutoff locations at the magnetic equator.

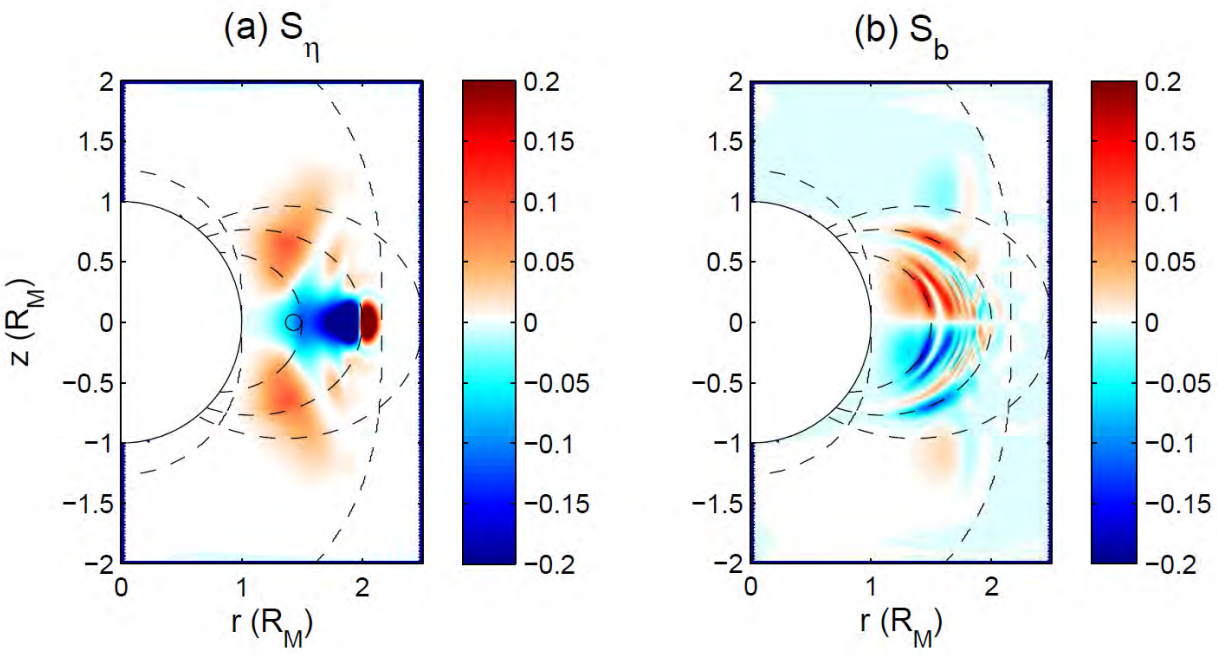

Figure 3. The Poynting flux S of wave (a) S_η. The positive direction is outward across the magnetic field line; and (a) S_b. The positive direction is south to north direction. The circle represent $\omega=\omega_{L0}$, the FW wave cutoff locations at the magnetic equator. In this figure, spatial structure of S_η are same as the FW structure shown in E_η and E_b, on the other hand, S_b clearly shows the fine structure of field-aligned IIH wave modes.

406

408

410

412 Media 1. Time dependent wave solution of $E(r,z,t) = E(r,z)\exp(-i\omega t)$; (a) E_η and (b) E_φ.

Princeton Plasma Physics Laboratory
Office of Reports and Publications

Managed by
Princeton University

under contract with the
U.S. Department of Energy
(DE-AC02-09CH11466)

P.O. Box 451, Princeton, NJ 08543
Phone: 609-243-2245
Fax: 609-243-2751

E-mail: publications@pppl.gov
Website: http://www.pppl.gov